J Appl Electrochem (2007) 37:991–1000
DOI 10.1007/s10800-007-9338-9

ORIGINAL PAPER

# Studies on electrodeposited nickel–yttria doped ceria composite coatings

**S. T. Aruna · V. K. William Grips · V. Ezhil Selvi · K. S. Rajam**

Received: 2 January 2007 / Revised: 24 April 2007 / Accepted: 1 May 2007 / Published online: 5 June 2007


**Abstract** Incorporation of ceria particles into the Ni matrix was found to improve the corrosion resistance of pure Ni coatings. With the aim of further improving the corrosion resistance of Ni-ceria, yttria was doped with ceria and used as distributed phase. About 8-mol% yttria doped ceria (8YDC) particles synthesized by a solution combustion process were dispersed in a nickel sulfamate bath and electrodeposition was carried out to prepare Ni–8YDC composite coatings at various current densities. The microhardness of the composite coatings was determined. Optical microscopy confirmed the incorporation of 8YDC particles into the Ni matrix. Potentiodynamic polarization and electrochemical impedance spectroscopy were used to characterize the corrosion behavior of the Ni–8YDC coatings. Scanning Electron Microscopy (SEM) and Energy Dispersive X-ray Analysis (EDAX) were used to characterize the corroded samples. The results were compared with those for Ni and Ni–$CeO_2$ coatings. The wear behavior of Ni–8YDC was studied. Wear tracks were characterized by MicroRaman Spectroscopy.

**Keywords** Corrosion · Composite coating · Nickel · Microhardness · Nanosize yttria doped ceria

## 1 Introduction

The need for electrodeposited composite coatings with improved resistance to highly aggressive environments is reaching new heights because of the growing demand for extended safe service life of industrial components. Many researchers have focused on the co-deposition of particles such as metallic powder, silicon carbides, oxides, polymer, diamond etc. [1–7] to improve the properties of the metal matrices. Since nickel is a strong, tough metal resistant to corrosion, erosion and abrasion, it has been widely used as the metal matrix. There are a number of methods of preparing particle dispersed metal matrix composites like metal infiltration, powder metallurgy or hot pressing [8]. However, the most common method is composite plating by electro [9] and electroless [10] plating techniques. The fabrication of nanocomposite films can also be achieved through electrochemical deposition of the matrix material from a solution containing a suspension of nanometer sized particles (e.g., ceramic, semiconductor, metal). These coatings exhibit unique mechanical, chemical and optical properties. For e.g., improved corrosion resistance of Ni coatings, on the incorporation of $Al_2O_3$ nanoparticles has been reported in the literature [11]. Xue et al. have reported lower wear and friction coefficient for Ni–$CeO_2$ compared to pure Ni [12].

The incorporation of ceria particles into the Ni matrix was found to enhance the corrosion resistance of Ni matrix [13]. It has been reported that addition of $Y_2O_3$ to metal hydride electrode diminishes the corrosion rate in Ni–MH batteries [14, 15]. Zhang and Li have reported enhanced mechanical and corrosion resistance of the Al matrix when 1% yttria particles were dispersed in Al matrix [16]. So it was interesting to study the mechanical, corrosion and wear resistance properties of a Ni composite coating containing particles of ceria doped with $Y_2O_3$. About 8 mol% Yttria doped ceria (8YDC) is one of the promising electrolyte used for intermediate temperature solid oxide fuel cells and this composition

S. T. Aruna (✉) · V. K. William Grips · V. Ezhil Selvi · K. S. Rajam
Surface Engineering Division, National Aerospace Laboratories, Post Bag No. 1779, Bangalore 560 017, India
e-mail: aruna_reddy@css.nal.res.in

was chosen as the dispersed phase. To the best of our knowledge, there are no reports on the preparation and properties of Ni-yttria doped ceria electrocomposite coatings and their corrosion behavior. In the present paper, the synthesis and properties of Ni-8 mol% yttria doped ceria (Ni-8YDC) nanocomposite coatings is presented. The corrosion and wear behaviors of Ni–8YDC coatings are compared with pure Ni and Ni–$CeO_2$ composite coatings.

## 2 Experimental

### 2.1 Combustion synthesis and characterization of 8YDC powder

About 8 mol% yttria doped ceria (8YDC) was synthesized by glycine nitrate combustion process using ceric ammonium nitrate as the oxidizer. About 1 g of $Y_2O_3$ was dissolved in warm dilute nitric acid to which 27.92 g of ceric ammonium nitrate $[(NH_4)_2Ce(NO_3)_6]$ and 10.7 g of glycine were added. The oxidizer to fuel ratio was maintained as unity based on the concept of propellant chemistry [17]. The starting solution was concentrated on a hot plate at about 300 °C until it formed a gel. As soon as the gel was completely dried a combustion reaction took place. Heat and gases were liberated during this reaction and an intense, self-sustained flame was formed, which rapidly propagated to the whole material resulting in the formation of a light yellow powder.

The crystallinity of the powder was identified by X-ray diffraction using a Rigaku X-ray diffractometer operated with $CuK_\alpha$ radiation. The crystallite size was determined using the Scherrer equation [18], $D = {}^{0.9\lambda}/_{\beta Cos\theta}$ where D is the crystallite size, $\lambda$ is the incident radiation wavelength (1.5418 Å for $CuK_\alpha$), $\beta$ is the corrected peak width at half-maximum intensity and $\theta$ is the angular position. The morphology of the as prepared powder was studied using SEM (Leo 440I). The average agglomerated particle size was measured using a photosize analyzer (Sedigraph-5100). The Raman spectra of ceria and 8YDC powders were recorded with a DILOR-JOBIN-YVON-SPEX (Paris, France) integrated Raman Spectrometer (Model Labram).

### 2.2 Preparation of Ni–8YDC nanocomposite coating and its characterization

Nickel sulfamate bath that yields low internal stress and good ductility Ni coatings was employed [19]. Its composition was 300 g $L^{-1}$ nickel sulfamate, 10 g $L^{-1}$ nickel chloride, 30 g $L^{-1}$ boric acid and 0.2 g $L^{-1}$ sodium lauryl sulfate (SLS) $[CH_3(CH_2)_{10}CH_2OSO_3Na]$. SLS is used as a surfactant which reduces the interfacial tension and avoids pit formation. The nanosize 8YDC powder was dispersed in the nickel sulfamate bath and magnetically stirred overnight (pre-conditioning step). The very high surface energy of nanoparticles will tend to agglomerate the nanoparticles in a highly conducting electrolyte. To avoid agglomeration, no special dispersing agent or ultrasonication was used except the preconditioning step. A bath loading of 100 g $L^{-1}$ 8YDC powder (powder density of 4.1691 g $cm^{-3}$) was used. Plating was carried out at ambient conditions (~30 °C) during electrodeposition and its pH was adjusted to four by the addition of sulfamic acid or basic nickel carbonate before carrying out electrodeposition. Boric acid is known for its buffering action at pH 4 and hence boric acid buffered sulfamate baths are operated at pH 4. A nickel strip and a brass plate were used as anode and cathode, respectively. The polished brass substrate of area 2.5 cm × 3.75 cm was degreased with acetone followed by cathodic cleaning in 10% NaOH and acid dipping in 25% $H_2SO_4$ and washed with distilled water. The electrodeposition was carried out using Aplab 7253 regulated DC power supply. The deposition time was adjusted to achieve equal deposit thickness values based on Faraday's law. The current densities and duration used for electrodeposition were as follows: 0.23 A $dm^{-2}$ for 20 h, 0.77 A $dm^{-2}$ for 6 h, 1.55 A $dm^{-2}$ for 3 h, 3.1 A $dm^{-2}$ for 1.5 h and 5.4 A $dm^{-2}$ for 52 min. The bath was stirred by a magnetic stirrer. A constant rotation speed of 300 rpm was maintained. The deposits were given a copper backup layer and cut into smaller pieces. These samples were then embedded in a Bakelite matrix and polished to a mirror like finish, using standard metallographic techniques, to obtain cross sectional samples for hardness and image analysis. Using VideoPro 32 software, histograms showing the percentage of particles versus the particle size were obtained. Microhardness indentations were made onto the cross-sections to avoid the effect of the substrate. The microhardness measurements were performed on a Buehler Microhardness Tester (Micromet 100) by applying 50 gf load. The final microhardness values quoted were an average of 10 measurements performed at different locations in the center section of each coatings cross-section.

To determine the volume fraction of particles codeposited, Ni–8YDC was electroplated on the stainless steel substrate and then peeled off. The electroformed strips were dissolved in 1:1 dilute nitric acid. The Ni matrix dissolved in dilute nitric acid leaving behind the particles. The 8YDC powder was separated by centrifugation and dried at 200 °C for 48 h. Using the weight of the dried powder the volume fraction of particles incorporated in the Ni matrix was calculated.

### 2.3 Potentiodynamic polarization and impedance studies of Ni, Ni–$CeO_2$ and Ni–8YDC coatings

For electrochemical studies a more active substrate, mild steel, (composition 0.37 wt% C, 0.25 wt% Si, 0.66 wt% Mn and 68.69 wt% Fe) was used. The electrochemical studies of Ni, Ni–$CeO_2$ and Ni–8YDC coated mild steel samples were conducted using anAutolab PG Stat-30 (Potentiostat/galvanostat) system. The bath used for electrodeposition of Ni–$CeO_2$ was the same as reported earlier [13]. In order to minimize the influence of coating thickness on the electrochemical measurement parameters, all the samples were deposited to have a similar thickness of 15 ± 1 μm. The electrodeposition was carried out at 1.55 A $dm^{-2}$ for 49 min. A conventional three electrode cell was used in which a platinum strip of 1-$cm^2$ area served as the counter electrode and Ag/AgCl, 3 M KCl electrode as the reference electrode. The test sample was placed in a Teflon sample holder and the surface area exposed to the corrosive medium was approximately 0.785 $cm^2$. Corrosion measurements were carried out in 3.5% NaCl aqueous solution at room temperature, non-stirred and free-air condition. In order to establish the open circuit potential prior to the measurements, the sample was immersed in the solution for about 45 min. Impedance measurements were conducted using a frequency response analyzer (FRA). The spectrum was recorded in the frequency range 10 mHz–100 kHz with data density of 5 points per decade. The applied alternating potential had root-mean-square amplitude of 10 mV on the $E_{OCP}$. After each experiment, the impedance data were displayed as Nyquist and Bode plots. The frequency dependence of the phase angle indicates whether one or more time constants occur, which can be used to determine the equivalent circuit parameters. The data were curve fitted and analyzed using the EQUIVCRT program. After the EIS measurements the system was allowed to attain the $E_{OCP.}$ A polarization curve was measured in the range –0.2 to 0.2 V at a constant scan rate of 1 mV $s^{-1}$. A Tafel plot was obtained from the electrochemical measurements. The free corrosion potential ($E_{corr}$) and corrosion current density ($i_{corr}$) were deduced from the Tafel plot. The microstructure and the components of the coatings before and after potentiodynamic polarization were studied using SEM (Leo 440I) with Energy Dispersive X-ray Analysis (EDAX) attachment.

### 2.4 Wear studies of Ni–8YDC coatings

In order to investigate the tribological performance of the Ni–8YDC coating, wear tests were conducted on a pin-on-disc tribometer (DUCOM, India) under ambient conditions of temperature and humidity (30 °C, 50%RH) with an applied load of 9.8 N. Wear experiments were undertaken for specimens in a semicircular pin of radius 6 mm coated with Ni–8YDC. All the depositions for wear tests were carried out at 1.55 A $dm^{-2}$ for 3 h (~40 μm). All wear tests were conducted at a wear track radius of 30 mm and 200 rpm (slide speed of 0.628 m $s^{-1}$) to get a constant sliding distance of 4525 m. The disc used was hardened EN 31 steel with a Vickers hardness of 750 HV. The coefficient of friction was calculated by dividing the friction force by the normal force, which was recorded by a personal computer. Each test was repeated three times and the average result was taken. Before and after the wear tests the specimens were cleaned by ultrasonication. Dry wiping was carried out during the experiment to eliminate accumulated wear particles on the wear track. The wear volume was calculated using the equation:

$$V = \pi\left[R^2(R-h) - \frac{1}{3}\left(R^3 - h^3\right)\right]$$

where R is the radius of the pin and h is the height loss of the pin. The wear coefficient was calculated using the Holm–Archard relationship [20, 21]. The wear loss on the disc in the wear track was determined using a Roughness tester (Model-Surftest 301, Mitutoyo, Japan). The Raman spectra of the discs and pins after the wear test were also recorded.

## 3 Results and discussion

### 3.1 Powder characterization

The combustion synthesized 8YDC powder was highly porous (Fig. 1) due to the evolution of large amounts of gas during the combustion reaction. The as-synthesized 8YDC powder was crystalline and exhibited a fluorite type cubic

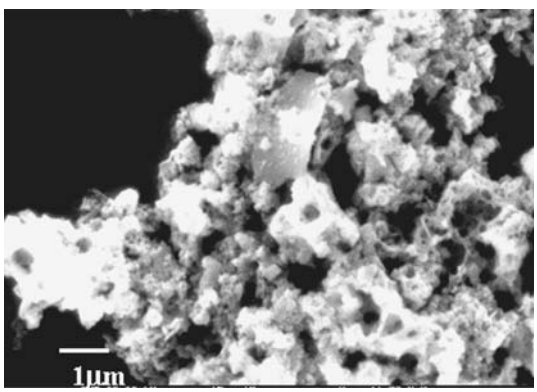


**Fig. 1** Scanning Electron Micrograph of as-synthesized 8YDC powder

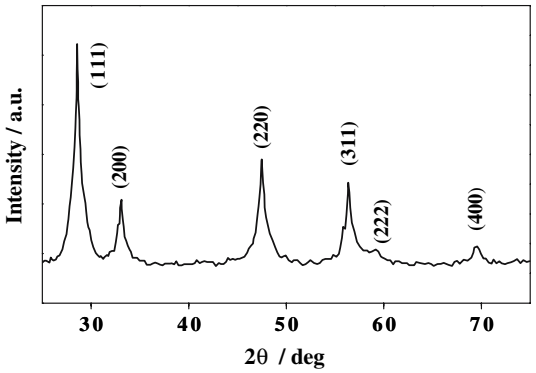


**Fig. 2** Powder XRD patterns of as-synthesized 8YDC powder

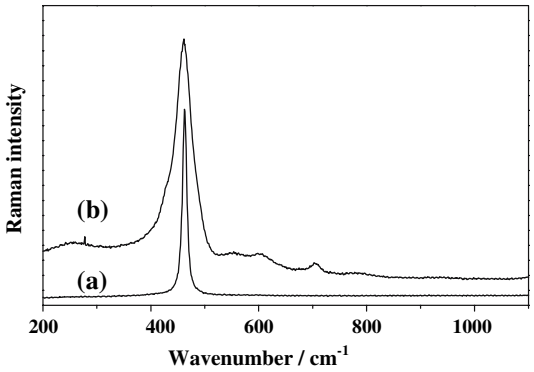


**Fig. 4** Raman spectra of (**a**) ceria and (**b**) 8YDC powders

structure (Fig. 2). The average crystallite size of 8YDC powder as calculated from XRD line broadening was 17 nm which is lower than that observed for pure ceria (22 nm). There was a slight decrease in the lattice parameter value of 8YDC (a = 0.54069 nm) compared to ceria (a = 0.541432 nm). The particle size distribution of the as-prepared particles (Fig. 3) shows that about 23 mass percent of the particles have size below 0.7 μm and there are quite a large amount of coarse particles with particle size as high as 30 μm. The average agglomerated particle size of 8YDC powder was 2.6 μm. The room temperature Raman spectra of ceria and 8YDC powders are shown in Fig. 4. Although they exhibit an intense $F_{2g}$ mode at about 465 $cm^{-1}$, 8YDC powder shows a broad band compared to ceria. Additional broad bands are also exhibited by 8YDC powder which may be attributed to the presence of oxygen vacancies [22].

### 3.2 Ni–8YDC coating characterization

The average Ni crystallite size calculated from X-ray line broadening for Ni–8YDC (1.55 A $dm^{-2}$) was 18 nm which is smaller than that of Ni–$CeO_2$ and Ni (30 and 36 nm respectively). It is evident from the XRD results that different particles will refine the nickel grain size to different extent. The probable mechanism involved in the co-deposition of particles during electrodeposition has been well documented [23]. The electrodeposition of Ni–8YDC coatings was not possible at higher current densities (>5.4 A $dm^{-2}$) as it resulted in the formation of a greenish powdery deposit and frothing was observed near the cathode during electrodeposition. At such conditions, the pH of the bath had increased from 4 to 5.6 during codeposition of 8YDC. It has been assumed that the formation of such powdery deposits and increase in pH are due to hydrogen discharge. With the consequent increase in pH at the cathode surface, metal hydroxide or basic salts are precipitated and become included in the deposit [24]. The XRD pattern of this greenish powdery deposit showed peaks corresponding to the cubic ceria phase. However, peaks corresponding to the formation of nickel hydroxide were not observed in the XRD pattern. The amount of nickel hydroxide precipitated may not be within the detectable limit. The EDAX analysis of the powdery deposit showed the presence of Ni, Ce, O and traces of S. The volume fraction of the particles incorporated into the Ni matrix as determined by gravimetric analysis for Ni–8YDC coatings was in the range 5–8%. In this range of 5–8% of 8YDC, the amount of $Y_2O_3$ in the composite will be in the range 1–3 wt%. The vol% of particles incorporated is higher in the lower current density region and vice versa. Yao et al have also observed lower content of co-deposited SiC nanoparticles at higher current density [25]. However, the current densities used by them were much higher (6–18 A $dm^{-2}$).

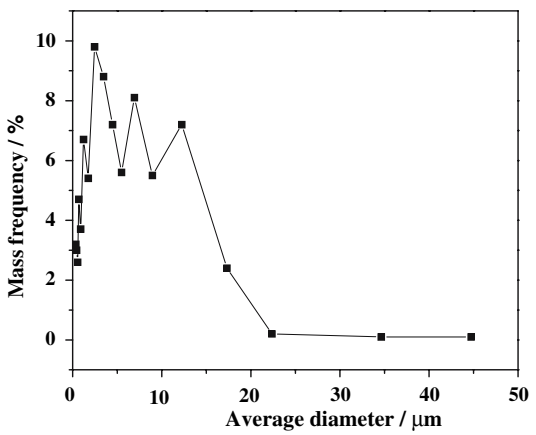


**Fig. 3** Particle size distribution of as-prepared 8YDC powder

There was an increase in the microhardness of the Ni matrix with the incorporation of 8YDC particles. The microhardness values of pure nickel, Ni–$CeO_2$ and Ni–8YDC coatings were in the range 320–360 HK, 380–514 HK and 400–500 HK respectively. Yttria doping in ceria and its incorporation in the Ni matrix did not significantly affect

the microhardness values of the composite coatings. Ni–8YDC followed the same trend in their microhardness values exhibiting maxima and minima similar to Ni–$CeO_2$ already reported [13]. The plot of microhardness versus applied current density of Ni–8YDC composite coating is shown in Fig. 5. The Ni–8YDC composite coating electrodeposited at 1.55 A $dm^{-2}$ exhibited similar microhardness values as that of Ni–$CeO_2$ and hence for corrosion and wear studies the electrodepositions were carried out at 1.55 A $dm^{-2}$. The enhancement in the microhardness of the Ni matrix is related to the dispersion strengthening effect caused by ceramic particles in the composite coatings, which impede the motion of dislocations in the metallic matrix [23].

The typical optical micrographs of the cross section of Ni–8YDC composite coating electrodeposited at 0.23 A $dm^{-2}$ shows well dispersed smaller 8YDC particles without much agglomeration (Fig. 6a(inset)) and the coating electrodeposited at 3.1 A $dm^{-2}$ contained larger agglomerated particles (Fig. 6b(inset)). This is an important observation and an attempt was made to understand this. This may be true for all kinds of particles with a wide range of distribution. The image analysis of the cross-section was used for generating the histograms. From the histogram (Fig. 6a) it can be seen that at 0.23 A $dm^{-2}$, the percentage of particles with the size range of 0.36 μm and below constitutes 30% and it becomes 60% for 0.6 μm and below size range. On the other hand, at highest current density (3.1 A $dm^{-2}$) the histogram (Fig. 6b) shows only 40% of the particles below 0.75 μm. It is clearly seen from this observation that at lower current density more finer particles are codeposited.

In the literature, for co-deposition process, five steps have been identified [26]. The last step is the adsorption of the ionic cloud at the cathode where particles are entrapped within the metal deposit. For a fixed stirring rate (rpm) the

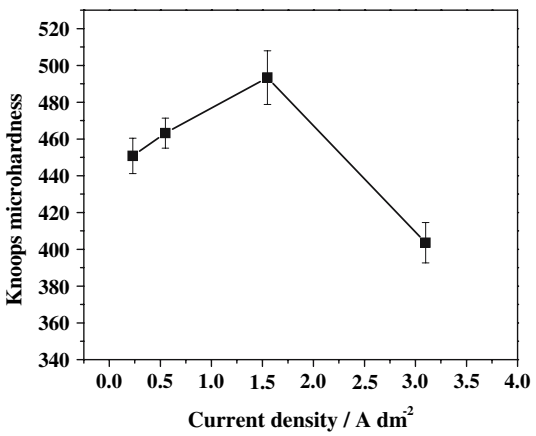


**Fig. 5** Plot of microhardness versus current density for Ni–8YDC composite coatings

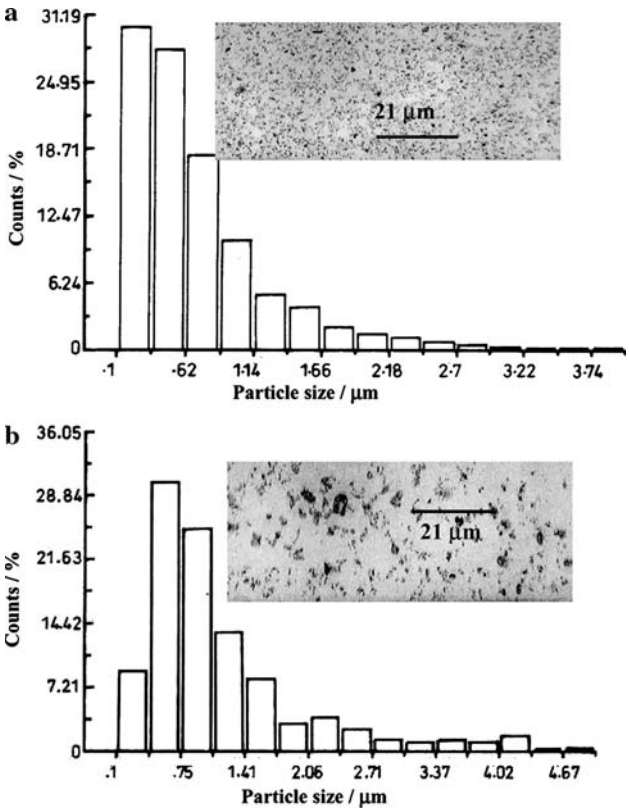


**Fig. 6** Histogram and Optical micrographs of Ni–8YDC coatings electrodeposited at (**a**) 0.23 A $dm^{-2}$ and (b) 3.1 A $dm^{-2}$

retention time of the particle in front of the cathode is same for all the current densities. At lower current densities, the rate of nickel deposition is lower and hence the probability of smaller size particles getting entrapped in the deposit is higher. At higher current densities the thickness of the nickel layer deposited is greater and the probability of retaining bigger particles in the growing deposit is also higher. This is schematically represented in Fig. 7.

Recently, researchers have shown interest in uniform and finer particle codeposition in metal matrices. There are reports on the use of pulsed current for selective entrapment of uniform sized particles with the larger particles being preferentially removed during the reverse pulse period to produce a finer deposit with lesser agglomeration [26]. Due to the pulse reversal in this case, the dissolution of metal matrix takes place and the coarser particles are removed. This method of plating has two disadvantages: (i) the plating rate is decreased due to the dissolution process, (ii) in some cases due to metal dissolution; passivation of metal occurs. However, in the present study with 8YDC particles it was observed that by applying a lower current density during DC electrodeposition a uniform distribution of smaller particles can be achieved without the use of an expensive pulsed power supply. The incorporation of finer particles with uniform distribution in the deposit depends

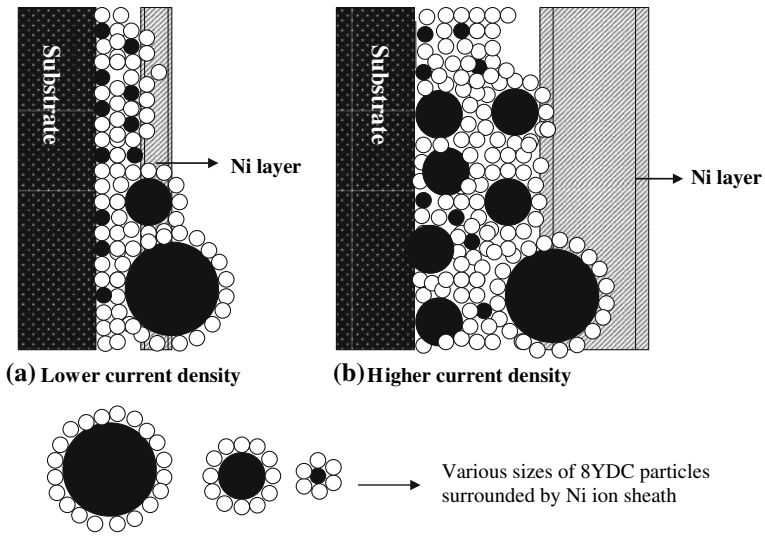


**Fig. 7** Schematic representation of the composite electrodeposition at (**a**) low current density and (**b**) high current density

on the starting particle size distribution, charge on the particles, and plating parameters like stirring speed, temperature, pH and current density. A systematic study of these variables can facilitate in the preparation of tailor made composite coatings containing different sized particles. A paper covering these aspects will be communicated soon.

### 3.3 Potentiodynamic polarization and impedance studies of Ni, Ni–$CeO_2$ and Ni–8YDC coatings

#### *3.3.1 Corrosion studies*

The electrochemical parameters obtained from the potentiodynamic polarization plots are listed in Table 1. The values reported are an average of four measurements. The corrosion potential of Ni–8YDC shifts more positive than Ni and Ni–$CeO_2$ indicating the nobler behavior of Ni–8YDC. The $i_{corr}$ value of Ni–8YDC was 0.16 μA $cm^{-2}$ as against 0.26 μA $cm^{-2}$ for Ni–$CeO_2$ and 0.61 μA $cm^{-2}$ for Ni. The polarization resistance also increased in the same order. The corrosion behavior of Ni, Ni–$CeO_2$ and Ni–8YDC were also investigated by impedance spectroscopy. Figure 8 shows the Nyquist plots of the coatings; they appear as single semicircles. At higher frequencies, interception with the real axis is ascribed to the electrolyte bulk resistance ($R_s$) and at low frequencies interception with the real axis is ascribed to the charge transfer resistance ($R_{ct}$). In the case of Ni coating, Warburg diffusion behavior was observed in the low frequency region supporting our earlier observation and the equivalent circuit for Ni coating was similar to that already reported [13]. The Nyquist plot of Ni observed in this study is similar to that reported by Benea et al. [27]. Figure 9 shows the impedance spectra of the three coatings in a Bode plot representation. The Bode plot (Phase angle versus log (freq)) of the Ni coating shows a single peak, which corresponds to the electrode/electrolyte interface. Bode plots of Ni–$CeO_2$ and Ni–8YDC show a broad peak representing two relaxation processes. The appropriate equivalent circuit used for fitting the parameters of Ni–8YDC is similar to that of Ni–$CeO_2$ [13]. The Ni coating showed the presence of the electrode/electrolyte interface with Warburg diffusion, whereas Ni–$CeO_2$ and Ni–8YDC coatings showed the presence of two interfaces; $R_{ct}$ and $Q_{dl}$ representing the electrode/electrolyte interface while $R_c$ and $Q_c$ corresponds to the coating electrolyte interface. The fitted values are tabulated in Table 2. From

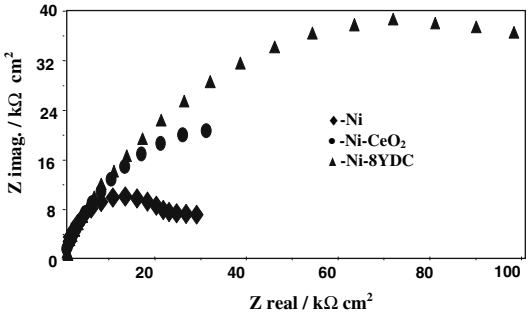


**Fig. 8** Nyquist plots of (**a**) Ni, (**b**) Ni–$CeO_2$ and (**c**) Ni–8YDC coatings

**Table 1** Corrosion potential, corrosion rates and Tafel slopes calculated from potentiodynamic diagrams for pure Ni, Ni–$CeO_2$ and Ni–8YDC coatings

| Sample | $i_{corr}$ (μA $cm^{-2}$) | $E_{corr}$ (V) | $b_c$ (V $dec^{-1}$) | $b_a$ (V $dec^{-1}$) | $R_p$ (Ω $cm^2$) |
|---|---|---|---|---|---|
| Ni | 0.61 | –0.298 | 0.078 | 0.130 | 35,940 |
| Ni–$CeO_2$ | 0.26 | –0.285 | 0.068 | 0.107 | 60,340 |
| Ni–8YDC | 0.16 | –0.284 | 0.108 | 0.079 | 1,18,000 |

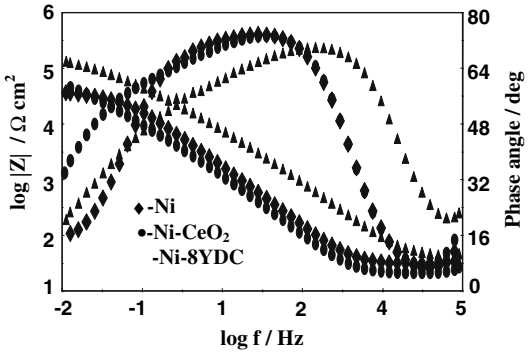


**Fig. 9** Bode plots of (**a**) Ni, (**b**) Ni–$CeO_2$ and (**c**) Ni–8YDC coatings

the electrochemical impedance study, the following two conclusions can be drawn: (i) there was an improvement in the corrosion resistance of Ni and Ni–$CeO_2$ compared to the previous coatings [13]. This is probably due to the greater thickness of the present coatings (15 μm) compared to the previous coatings (11 μm). (ii) Among the three coatings studied in the present study, Ni–8YDC showed the highest corrosion resistance.

Szczygiel and Kolodziej have reported that $Al_2O_3$ particles facilitate the formation of a passive layer on the nickel surface the finer they are [28]. The non-conducting particles have a screening effect and if they are homogeneously distributed in the nickel matrix, they reduce the area of contact between the matrix and the corroding solution. For this reason, the corrosion resistance of the composite coatings with smaller the particles in size and their uniform distribution [28]. In the present investigation, $CeO_2$ and 8YDC particles were found to improve the corrosion resistance of Ni coating. These particles being oxide ceramic particles the above reasoning holds good for their improved corrosion resistance. Both Ni–$CeO_2$ and Ni–8YDC show uniform distribution of particles but the Ni–$CeO_2$ coating contains a higher area fraction of particles (~22%) compared to Ni–8YDC (~15%) (Fig. 10a, b). Although the Ni–8YDC coating contained lower area fraction of particles it showed improved corrosion resistance. This may be attributed to the intrinsic property of $Y_2O_3$ doped ceria. It has also been reported that the incorporation of 1 wt% $Y_2O_3$ improved the corrosion resistance of Al matrix prepared by rapid solidification [16] which confirms our observation of improved corrosion resistance of 8YDC in the Ni matrix.

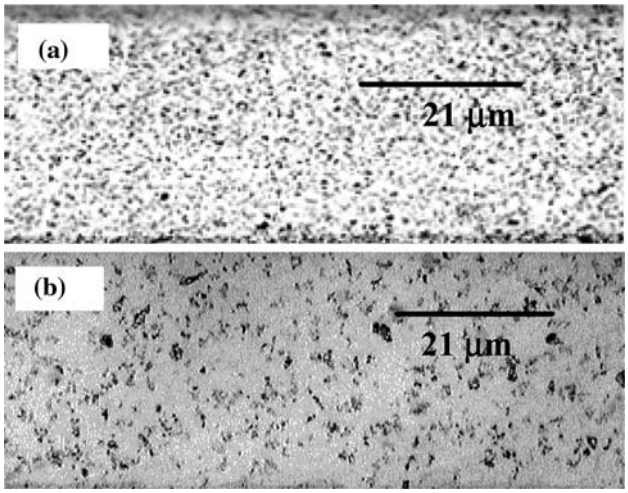


**Fig. 10** Optical micrographs of the cross-section of (**a**) Ni–$CeO_2$ (after Ref. 13, Fig. 7b) and (**b**) Ni–8YDC electrodeposited at 1.55 A $0dm^{-2}$

The XRD studies indicated the presence of smaller Ni crystallites in Ni–8YDC (18 nm) compared to Ni–$CeO_2$ (27 nm) and also smaller crystallite size for 8YDC particles. This would also have contributed to the improved corrosion resistance of Ni–8YDC. Mishra and Balasubramaniam have also reported similar observations on the basis of their study on the effect of nanocrystalline nickel of different grain sizes (8–28 nm) on the corrosion resistance in 1 mol% $H_2SO_4$ [29].

### *3.3.2 SEM studies*

The SEM of the surface topography of plain Ni coating showed the presence of irregular shaped larger grains (Fig. 11). SEM of the surface topography of corroded samples showed the presence of a fine grained Ni matrix in Ni–8YDC (Fig. 12). These irregular shaped grains transform to spherical smaller grains upon incorporation in Ni matrix. The enhanced corrosion resistance of Ni–8YDC may be due to the finely crystalline nature of the Ni grains. The EDAX of corroded Ni sample showed a higher percentage of Fe (4%), whereas Ni–$CeO_2$ and Ni–8YDC composite coatings showed lower Fe % (0.39% and 0.16% respectively). The EDAX carried out on the white spots showed 28 and 30% of Ce respectively, for the corroded Ni–$CeO_2$ and Ni–8YDC composite coatings.

**Table 2** Electrochemical impedance analysis data

| Type of coating | $R_S$ (Ω $cm^2$) | $Q_c$ (μF $cm^{-2}$) | $R_c$ (kΩ $cm^2$) | $Q_{dl}$ (μF $cm^{-2}$) | $R_{ct}$ (kΩ $cm^2$) | W ($\mu\Omega$ $cm^2$ $s^{0.5}$) |
|---|---|---|---|---|---|---|
| MS/Ni | 10 | 8.20 | 5.30 | 5.97 | 28 | 855 |
| MS/Ni–$CeO_2$ | 11 | 6.68 | 14.80 | 2.63 | 67 | – |
| MS/Ni–8YDC | 13 | 0.87 | 86.35 | 0.07 | 109 | – |

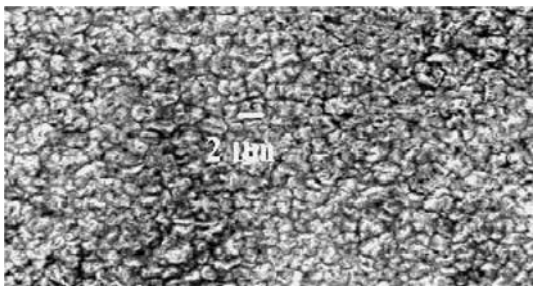


**Fig. 11** Scanning Electron Micrograph of surface topography of Ni coating on mild steel after potentiodynamic polarization studies

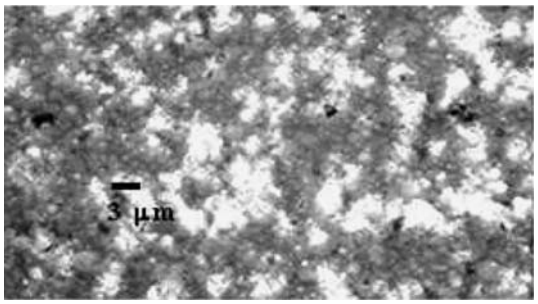


**Fig. 12** Scanning Electron Micrograph of surface topography of Ni–8YDC coating after potentiodynamic polarization studies

### *3.3.3 Wear studies*

It was observed in our previous study that the average coefficient of friction for Ni and Ni–$CeO_2$ coatings were 0.517 and 0.374 respectively [13]. For Ni–8YDC the coefficient of friction oscillated between 0.5 and 0.7 with an average of 0.54 (Fig. 13). The higher coefficient of friction for Ni–8YDC shows that there is a change in the polishing nature of ceria particles on doping yttria. The morphology of the typical wear tracks of the pins (coated with Ni, Ni–$CeO_2$ and Ni–8YDC) and their counter faces (discs) are shown in Fig. 14. The wear tracks on the pins showed grooves parallel to the direction of motion for all the three samples. The number of grooves was more for Ni (Fig. 14a) compared to Ni with particles (Fig. 14c and 14e), and it was least for the coating containing 8YDC particles (Fig. 14e). The groove depth of the wear tracks on the disc (Fig. 14d and 14f) was more for composite coatings due to the presence of particles. In the case of the wear track of the disc (Fig. 14b) used for testing the Ni coated pin, some material (wear debris) transfer from the pin to the adjacent areas of the track was seen. Delamination was observed on the wear tracks of pins for the composites (Fig. 14c and e) and it was greater for the coating containing ceria particles (Fig. 14e). This is also reflected in the wear volume loss of Ni–$CeO_2$. The wear volumes for

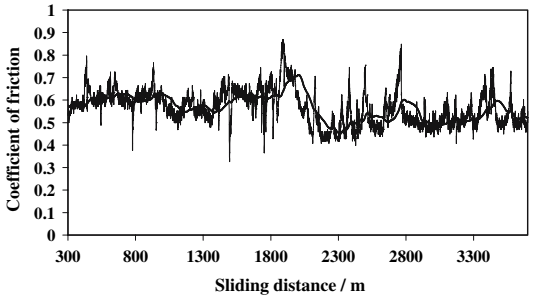


**Fig. 13** Plot of coefficient of friction versus sliding distance for Ni–8YDC coated samples

Ni, Ni–$CeO_2$ and Ni–8YDC were $4.583 \times 10^{-3}$, $5.481 \times 10^{-3}$, and $4.237 \times 10^{-3}$ $mm^3$ respectively. At higher magnifications (Fig. 15a and b), the grooves of the wear tracks of the pins of Ni–$CeO_2$ and Ni–8YDC indicate more delaminated areas for the former. This observation also indicates that the doping of yttria in ceria has changed the wear behavior. Film formation on the wear tracks of the discs rubbed against the composite coatings was observed and the same was absent on the disc used against the Ni coated pin. The Raman spectra of the Ni–8YDC transferred disc did not show the presence of a 465 $cm^{-1}$ peak corresponding to the $F_{2g}$ mode typical of a fluorite-based system (Fig. 16). However, it showed a broad band between 550 and 750 $cm^{-1}$ in the Raman spectra. The wear coefficients calculated for Ni–8YDC was $4.46 \times 10^{-7}$ and for Ni–$CeO_2$ and Ni it has been already reported as $5.10 \times 10^{-7}$ and $3.94 \times 10^{-7}$, respectively. These values indicate that all the coatings have undergone mild adhesive wear of a burnishing type [30].

## 4 Conclusions

Nanosize (17 nm) 8YDC particles prepared by the glycine–nitrate combustion route were incorporated in a nickel matrix. Ni–8YDC composite coatings containing small particles with uniform distribution were achieved by DC electroplating at low current density. An attempt was made to explain this schematically. Ni–8YDC and Ni–$CeO_2$ composite coatings exhibited similar microhardness values at a current density of 1.55 A $dm^{-2}$. Corrosion testing confirmed the improved resistance of Ni–8YDC coatings compared to Ni–$CeO_2$ and Ni in the 3.5% NaCl solution. SEM of corroded surfaces showed the presence of very fine nickel grains in the case of Ni–8YDC which resulted in higher corrosion resistance. The EDAX also confirmed the lower % of Fe in Ni–8YDC. The improved corrosion resistance of Ni–8YDC was attributed to (i) the smaller crystallite sizes of 8YDC

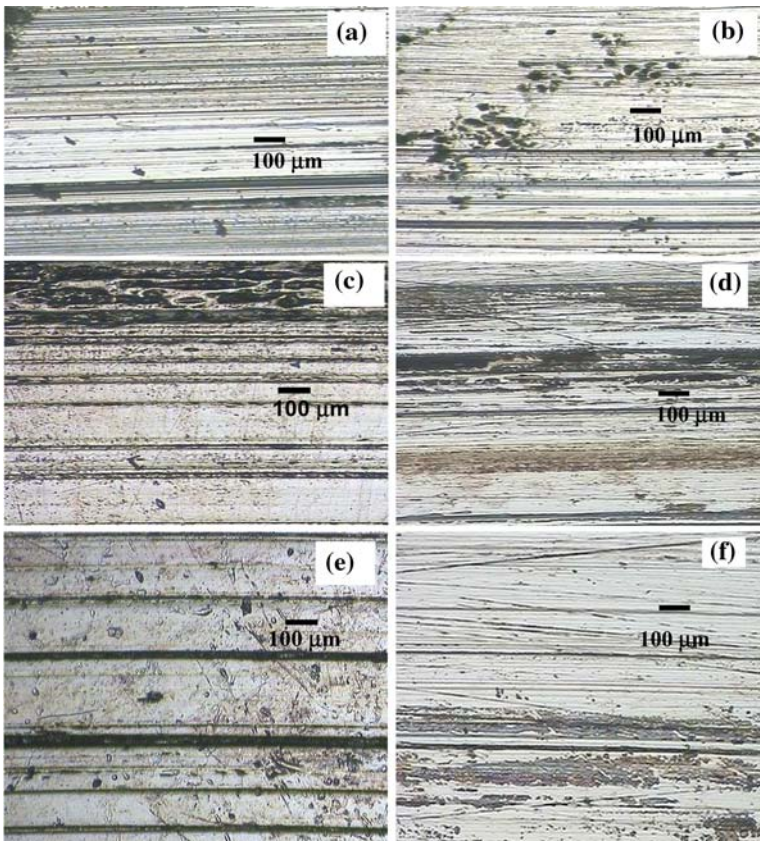


**Fig. 14** Optical micrographs of the wear tracks of the pins coated with (**a**) Ni, (**c**) Ni–$CeO_2$ and (**e**) Ni–8YDC after wear tests and (**b**), (**d**) (**f**) are their corresponding wear tracks on discs

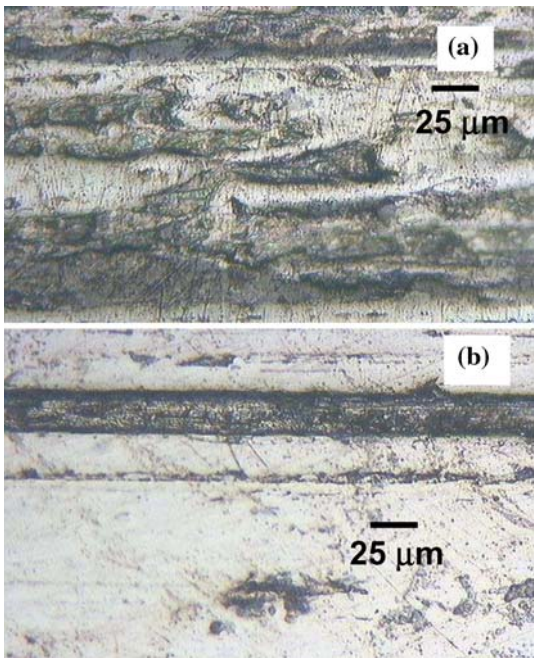


**Fig. 15** Optical micrographs of the wear track of the coated pins (**a**) Ni–$CeO_2$ and (**b**) Ni–8YDC at higher magnifications

particles, (ii) finer Ni crystallites and (iii) the effect of doping of yttria. Wear studies showed mild adhesive wear of burnishing type for all the coatings.

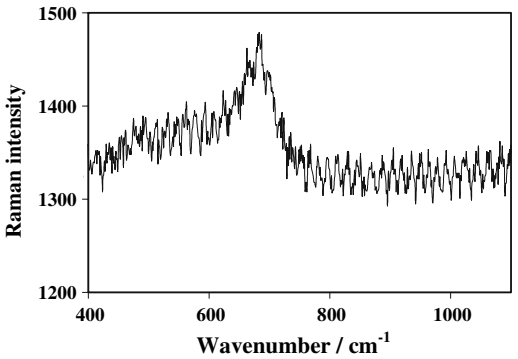


**Fig. 16** Raman spectra of wear tracks of the disc after wear testing tested with Ni–8YDC coated pins

**Acknowledgements** The authors gratefully acknowledge financial support received from the CSIR Task force program on ''Custom tailored special materials''. The authors thank the Director, NAL for permission to publish this work. The authors also thank Ms. C. N. Bindu for help in carrying out some of the experiments. The authors are thankful to Mr. Siju for the microhardness measurements, Mr. Venkataswamy for the SEM and Dr. Anjana Jain for the XRD measurements.

## References

1. Powel BR, Bloink RL, Erkel CC (1988) J Am Ceram Soc 71:C104

2. Moller A, Hahn H (1999) Nanostruct Mater 12:259
3. Müller B, Ferkel H (1999) Z Metallkd 90:868
4. Shao I, Vereecken PM, Chien CL, Searson PC, Cammarata RC (2002) J Mater Res 17:1412
5. Zhou M, de Tacconi NR, Rajeshwar K (1997) J Electroanal Chem 421:111
6. Benea L, Borello PL, Martelli S (2002) Wear 249:995
7. Xu H, Yang Z, Li M-K, Shi Y-L, Huang Y, Li H-L (2005) Surf Coat Technol 191:161
8. Balathandan S, Seshadri SK (1992) Met Finish 90:51
9. Gyftou P, Stroumbouli M, Pavlatou EA, Asimidis P, Spyrellis N (2005) Electrochim Acta 50:4544
10. Balaraju JN, Kalavati, Rajam KS (2006) Surf Coat Technol 200:3933
11. Szczygiel B, Kolodziej M (2005) Electrochim Acta 50:4188
12. Xue Y-J, Jia X-Z, Zhou Y-W, Ma W, Li J-S (2006) Surf Coat Technol 200:5677
13. Aruna ST, Bindu CN, Ezhil Selvi V, William Grips VK, Rajam KS (2006) Surf Coat Technol 200:6871
14. Kaiya H, Ookawa T (1995) J Alloys Compd 231:598
15. Maurel F, Leblanc P, Knosp B, Backaus-Ricoult M (2000) J Alloys Compd 309:88
16. Zhang T, Li DY (2001) Wear 251:1250
17. Patil KC, Aruna ST, Ekambaram S (1997) Curr Opin Solid State Mater Sci 2:158
18. Klug H, Alexander L (1974) X-ray diffraction procedures for polycrystalline and amorphous materials. John Wiley, New York
19. Tsuru Y, Nomura M, Foulkes FR (2000) J Appl Electrochem 30:231
20. Holm R (1946) Electric contacts. Almquist and Wiksells, Stockholm, Section 40
21. Archard JF (1953) J Appl Phys 24:981
22. Zha S, Fu Q, Lang Y, Xia C, Meng G (2001) Mater Lett 47:351
23. Buelens C, Fransaer J, Celis JP, Roos JR (1992) Bull Electrochem 8:371
24. Lyons EH Jr (1963) In: Lowenheim FA (ed) Modern electroplating. John Wiley & Sons Inc, New York, pp 23
25. Yao Y, Yao S, Zhang L, Wang H (2007) Mater Lett 61:67
26. Low CTJ, Wills RGA, Walsh FC (2006) Surf Coat Technol 201:371
27. Benea L, Bonora PL, Borello A, Martelli S (2002) Mater Corros 53:23
28. Szczygiel B, Kolodziej M (2005) Trans Inst Met Finish 83:181
29. Mishra R, Balasubramaniam R (2004) Corros Sci 46:3019
30. Rabinowicz E (1984) Wear 100:533